

Vaccination-transmission coupled mechanism based on parallel minority game

Chenli Xue(薛琛丽), Xiaofeng Luo(罗晓峰), and Gui-Quan Sun(孙桂全)
Citation: Chin. Phys. B, 2026, 35 (**2**): 028705. DOI: 10.1088/1674-1056/ae306a
http://cpb.iphy.ac.cn; http://iopscience.iop.org/cpb

What follows is a list of articles you may be interested in

Impact of message fatigue and individual behavioral responses on epidemiological spread in temporal simplicial networks

Xiao-Nan Fan(樊晓楠) and Xuemei You(由雪梅)
Chin. Phys. B, 2025, 34 (**3**): 038703. DOI: 10.1088/1674-1056/adaade

Epidemic threshold influenced by non-pharmaceutical interventions in residential university environments

Zechao Lu(卢泽超), Shengmei Zhao(赵生妹), Huazhong Shu(束华中), and Long-Yan Gong(巩龙延)
Chin. Phys. B, 2024, 33 (**2**): 028707. DOI: 10.1088/1674-1056/ace2b0

Stability and optimal control for delayed rumor-spreading model with nonlinear incidence over heterogeneous networks

Xupeng Luo(罗续鹏), Haijun Jiang(蒋海军), Shanshan Chen(陈珊珊), and Jiarong Li(李佳容)
Chin. Phys. B, 2023, 32 (**5**): 058702. DOI: 10.1088/1674-1056/acb490

Effective suppression of beta oscillation in Parkinsonian state via a noisy direct delayed feedback control scheme

Hai-Tao Yu(于海涛), Zi-Han Meng(孟紫寒), Chen Liu(刘晨), Jiang Wang(王江), and Jing Liu(刘静)
Chin. Phys. B, 2021, 30 (**3**): 038703. DOI: 10.1088/1674-1056/abd395

Computational study of non-catalytic T-loop pocket on CDK proteins for drug development

Huiwen Wang(王慧雯), Kaili Wang(王凯丽), Zeyu Guan(管泽雨), Yiren Jian(简弋人), Ya Jia(贾亚), Fatah Kashanchi, Chen Zeng(曾辰), Yunjie Zhao(赵蕴杰)
Chin. Phys. B, 2017, 26 (**12**): 128702. DOI: 10.1088/1674-1056/26/12/128702

Vaccination-transmission coupled mechanism based on parallel minority game

Chenli Xue(薛琛丽)[1], Xiaofeng Luo(罗晓峰)[1,†], and Gui-Quan Sun(孙桂全)[1,2,‡]

[1] *School of Mathematics, North University of China, Taiyuan* 030051, *China*
[2] *Complex Systems Research Center, Shanxi University, Taiyuan* 030006, *China*

(Received 16 October 2025; revised manuscript received 19 December 2025; accepted manuscript online 23 December 2025)

Vaccination is a key strategy to curb the spread of epidemics. Heterologous vaccination, unlike homologous vaccination which acts on a single target and forms a single immune barrier, covers multiple targets for broader protection. Yet, heterologous vaccination involves a complex decision process that conventional game-theoretic approaches, such as classical, evolutionary, and minority games cannot adequately capture. The parallel minority game (PMG) can handle bounded-rational, multi-choice decisions, but its application in vaccine research remains rare. In this study, we propose a vaccination-transmission coupled dynamic mechanism based on the parallel minority game and simulate it on a two-dimensional lattice. Using actual observational data and a mean-field mathematical model, we verify the effectiveness of this mechanism in simulating realistic vaccination behavior and transmission dynamics. We further analyze the impact of key parameters, such as vaccine efficacy differences and the proportion of individuals eligible for vaccine switching, on containment effectiveness. Our results demonstrate that heterologous vaccination surpasses homologous vaccination in containment effectiveness, particularly when vaccine efficacy varies significantly. This work provides a novel framework and empirical evidence for understanding individual decision-making and population-wide immunity formation in multi-vaccine settings.

Keywords: infectious disease modeling, basic reproduction number, parallel minority game, heterologous vaccination

PACS: 87.19.X–, 87.23.Ge, 89.75.–k

DOI: 10.1088/1674-1056/ae306a **CSTR:** 32038.14.CPB.ae306a

1. Introduction

Vaccination is a crucial measure for interrupting viral transmission and establishing herd immunity, and it has played a decisive role in controlling and even eradicating severe infectious diseases such as smallpox throughout human history.[1–4] Since the COVID-19 pandemic began, vaccines based on multiple technological platforms have been developed. The traditional homologous vaccination (Homo) strategy, in which both primary and booster immunizations rely on the same platform, targets only a single site of action. As a result, it creates a relatively uniform immune barrier in the population and shows limitations in protective efficacy.[5,6] In this context, heterologous vaccination (Hetero) strategy (i.e., alternating vaccines based on different technological platforms) has emerged as a significant research focus, as it can provide protection against multiple targets and thereby establish a more comprehensive and integrated immune barrier in the population.[7–9] Compared with homologous vaccination, heterologous vaccination involves greater decision-making complexity, which raises the question of how individual vaccination choices influence epidemic dynamics and the underlying mechanisms in environments where multiple vaccines coexist.[10–12]

In studies of infectious disease transmission dynamics, existing models commonly use fixed vaccination rates or simple assumptions to describe immunization behavior. For instance, the classical population dynamics model developed by Anderson and May treats vaccination rates as input parameters to derive population immunity thresholds and evaluate the effectiveness of outbreak control.[13] Hethcote also emphasized in his review the decisive role of vaccination coverage in outbreak control, but did not consider the dynamic feedback of individual behavior.[14] Diekmann *et al.* then further refined the theoretical link between inoculation rates and conditions for outbreak abatement by defining the basic regeneration number mathematically.[15] Recently, Ferguson *et al.*,[16] Zheng *et al.*,[17] and Moghadas *et al.*[18] conducted scenario modelling of outbreak trends under different vaccination rates, again assuming vaccine coverage to be exogenously given. Although these studies have made important progress in elucidating the macroscopic relationship between vaccination levels and outbreak evolution, the results make it difficult to explain the complex transmission patterns arising from vaccine hesitancy and changes in risk perceptions in reality. They fail to account for the dynamic adjustments in decision-making that arise from bounded rationality and be-

†Corresponding author. E-mail: luoxiaofeng@nuc.edu.cn
‡Corresponding author. E-mail: gquansun@126.com

© 2026 Chinese Physical Society and IOP Publishing Ltd. All rights, including for text and data mining, AI training, and similar technologies, are reserved.

havioral heterogeneity.[19–22]

To remedy these shortcomings, researchers have introduced game theory into infectious disease research.[23] Classical game theory usually assumes that individuals are perfectly rational and choose the optimal strategy through cost-benefit analysis. For example, Bauch and Earn[19] and Galvani *et al.*[24] studied the impact of self-interested behavior on vaccination coverage and pointed out that free-riding can lead to insufficient herd immunity; Perisic and Bauch[25] analyzed the effects of intervention strategies. However, classical game theory assumes perfect information and optimal decision-making, which can hardly reflect the bounded rationality and cognitive constraints of individuals in reality.[26,27] To address the limitations of the perfect rationality assumption, evolutionary game theory introduces strategy imitation and group learning to portray the dynamic evolution of boundedly rational behavior. For example, Reluga,[20] Fu *et al.*,[28] and Bauch and Bhattacharyya[29] investigated the evolution of vaccination strategies in dynamic or networked environments, respectively, and revealed the impact of individual strategy adjustments over time on outbreak fluctuations. However, evolutionary game theory often leads to "majority strategy dominance", making it difficult to explain the heterogeneity and diversity of inoculation behaviors.[30–32] In addition, the minority game emphasizes that in a competitive resource environment, individuals choosing a minority strategy can achieve higher returns, as studied by Challet and Zhang,[33] Zhang *et al.*,[34] De Martino *et al.*[35] However, its basic setup is only confined to two-choice scenarios and cannot directly portray the complex decision-making of multiple vaccines coexisting. In summary, although these studies have made progress in revealing the relationship between vaccination behavior and outbreak transmission, there are still shortcomings in portraying the decision-making mechanisms of boundedly rational individuals under multi-vaccine scenarios. Parallel minority game (PMG), as an extension of the minority game, can deal with multi-strategy choice problems,[36–38] which can handle the decision-making behaviors of individuals in real-life limited rationality (incomplete information and limited capacity to process information) as well as multi-vaccine choice scenarios.

Motivated by these two aspects, this paper constructs a coupled framework of vaccination-transmission based on a parallel minority game. Within this framework, we simulate the spread of infectious diseases on a two-dimensional lattice and, based on the simulation results, conduct a comparative analysis of three vaccination strategies: homologous vaccination (Homo), stochastic heterologous vaccination (Stoch-Hetero), and completely random heterologous vaccination (Rand-Hetero). We establish a mean-field mathematical model to characterize the average population-level dynamics, conduct theoretical analysis, and validate the efficacy of the vaccination-transmission mechanism, thereby achieving a coupling between micro-level individual decision-making and macro-level transmission dynamics. The findings indicate that heterologous vaccination strategies yield superior overall epidemic control outcomes compared to homologous vaccination. This research integrates complex behavioral decision-making with disease transmission dynamics. It provides an analytical framework for studying how boundedly rational individual choices affect disease spread in multi-vaccine environments.

The structure and organization of this article are as follows. In Section 2, we construct a vaccination decision-making mechanism based on the parallel minority game, establishing a coupled framework of individual decision-making and disease transmission. In Section 3, we first validate the accuracy of the proposed mechanism by comparing its simulation results with actual observational data. We then analyze the impacts of three key factors on prevention and control effectiveness: the difference in vaccine efficacy, the proportion h of individuals allowed to switch vaccines, and the vaccine efficacy in the primary immunization phase. In Section 4, we establish a mean-field mathematical model and conduct theoretical analysis. Furthermore, we validate the accuracy of the mechanism through the solution of the mathematical model. In Section 5, we summarize research findings, discuss the limitations of this work, and propose potential avenues for future research expansion.

2. The coupled vaccination-transmission framework based on the parallel minority game

During the COVID-19 pandemic, the emergence of multi-type vaccines based on multiple technological platforms has posed new challenges to traditional homologous vaccination (i.e., using the same vaccine type for both primary and booster immunizations, as illustrated by the blue individuals receiving "Vaccine A+A" in Fig. 1). Different vaccines enhance resistance of different target sites to viruses.[39] As shown in Fig. 1(a), when the population is primarily vaccinated with the same vaccine, the resulting immune barrier is relatively homogeneous. The virus may then target other sites to breach this relatively uniform immune barrier, ultimately leading to an expansion of the infection scale. To address this issue, many countries have adopted a heterologous vaccination strategy. This approach uses different vaccine types in the primary and booster stages, as shown by the green and magenta individuals in Fig. 1(b). It enhances multi-target resistance and establishes a more comprehensive immune barrier, thereby significantly improving protective efficacy. Existing clinical trials indicate that heterologous vaccination generally yields superior population protection compared to homologous vaccination.[40–42]

However, current clinical research remains insufficient in elucidating the underlying mechanisms, failing to clearly demonstrate the intrinsic relationship between individual vaccination decisions and herd immunity outcomes.

Although heterologous vaccination compensates for the limitations of homologous vaccination and provides more choices, individuals are bounded by "bounded rationality" (i.e., incomplete information and limited information-processing capacity) in their actual decision-making. Therefore, it is difficult for them to make a truly optimal choice among the types of vaccines available. As shown in Fig. 1(b), the decision-pending (orange) individuals are actually in a complex game situation when faced with multiple vaccine choices. They must choose one from multiple vaccine types, assessing the actual protective efficacy of different vaccines based on limited information and predicting others' selection preferences. This is in order to anticipate individual selection trends, thereby avoiding potential risks arising from the majority flocking to choose the mainstream vaccine (Vaccine A).

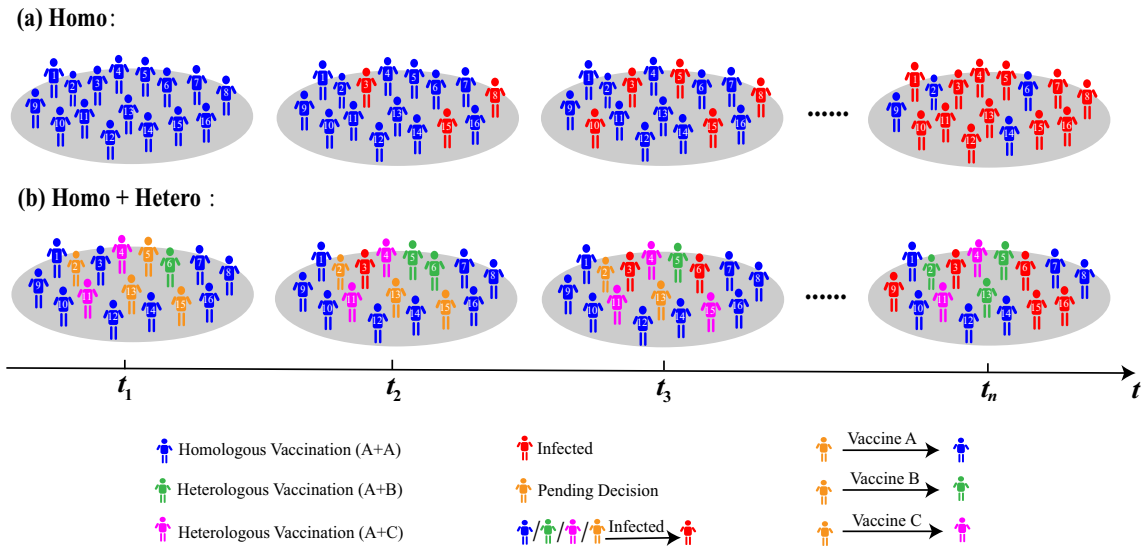


Fig. 1. Schematic illustration of epidemic dynamics under different vaccination strategies. (a) Homologous vaccination (Homo): all individuals receive the same type of vaccine (A+A), resulting in a larger final infection scale. (b) Mixed vaccination strategy (Homo+Hetero): an adaptive subpopulation (orange) dynamically chooses a booster (A+A, A+B, or A+C), reducing both the infection peak and final scale. The recovered compartment is omitted for simplicity. Colors denote states: blue (homogenously vaccinated), green/magenta (heterogeneously vaccinated), red (infected), orange (decision-pending).

Specifically, if the target site of the virus changes beyond the efficacy range of Vaccine A, those who selected Vaccine B (which operates via a different mechanism) would still retain effective immune protection. This dynamic decision-making process is difficult to capture accurately with three conventional game theories: classical game theory, evolutionary game theory, and minority game theory. Classical game theory assumes perfect rationality, meaning that individuals possess full information and strong processing capability, which does not match the reality of the above vaccine selection. Evolutionary game theory emphasizes the dominance of mainstream choices, while the minority game is limited to binary decisions. In contrast, the parallel minority game describes a scenario where some individuals, when faced with multiple choices, proactively avoid the majority-crowded option and instead adopt minority strategies to obtain higher payoffs. This majority avoidance mechanism aligns with some individuals actively choosing non-mainstream vaccines (such as Vaccine B) to counter the risk of a single-immunity barrier posed by mainstream vaccines (such as Vaccine A). Therefore, this study employs the parallel minority game to characterize individual decision-making in heterologous vaccination. Next, we elaborate on how this game framework simulates the dynamic vaccination decision process by defining local interaction rules and probabilistic selection mechanisms on a regular lattice network.

2.1. The coupled vaccination-transmission process

In the following, we first describe the grid structure and the definition of individual states. Let a two-dimensional space be discretized into a square grid of size $L \times L$, with the coordinate set $\{(i, j) \mid i, j = 1, 2, \ldots, L\}$. The grid thus contains L^2 cells. Assuming that the total number of individuals is N, the population density, denoted by the parameter ρ, is satisfied:

$$\rho = \frac{N}{L^2}, \quad (0 < \rho \leq 1). \tag{1}$$

This parameter controls the sparsity of individuals in the grid (specific values are provided in Subsection 2.2.1).

During the initialization stage, N individuals are placed on the grid by uniformly and non-repetitively sampling N cells from the total L^2 cells. Unoccupied cells are considered empty and do not participate in disease transmission. At

any time t, an individual $X_i(t)$ can be in one of four states: $X_i(t) \in \{S, I, R, V\}$, $i = 1, 2, \ldots, N$, where S represents susceptible, I infected, R recovered, and V vaccinated. This random initialization rule applies to all types of individuals, including the decision-making individuals (in orange) illustrated in Fig. 1.

The parallel minority game represents a variant of the minority game. The minority game originates from the "bar problem", where all individuals $i = 1, 2, \ldots, N$ choose from a common binary strategy set $A = \{a_1, a_2\}$ with the goal of selecting the strategy chosen by the minority to obtain a payoff. In the parallel minority game, the global strategy set is extended to $A = \{a_1, a_2, \ldots, a_D \mid D > 2\}$. Each individual i does not face the complete global set A when making decisions, but is instead assigned a unique local binary strategy subset $A_i \subset A$, where $|A_i| = 2$. Consequently, the actual choice range for each individual i is their specific $A_i = \{A_m, A_n\}$, where $m, n \in \{1, \ldots, D\}$ and $m \neq n$. The individual's decision objective accordingly shifts: the goal is no longer to be in the minority within the global strategy set A, but rather to select the strategy that is expected to be chosen by fewer participants within their own assigned local binary options A_i.

In a vaccination scenario, individuals face a total number of vaccine types $D > 2$. However, each individual chooses only between two available vaccines during decision-making, aiming to join the minority with lower infection risk between these two options.. This micro-level decision mechanism interacts with macro-level transmission dynamics through the following coupling process: individual vaccination choices directly drive disease spread, while transmission dynamics in turn shape subsequent vaccination decisions, forming a closed-loop feedback mechanism. Vaccination strategies serve as the starting point for individual decision-making. We first define the following three vaccination strategies.

1. Homologous vaccination (Homo) All individuals receive the same vaccine type for both primary and booster doses.

2. Heterologous vaccination (Hetero) Some individuals (proportion h) received different vaccines during the primary and booster phases of immunization. Based on the differing decision-making mechanisms in actual vaccination practices, they are further categorized into the following two types.

(i) Stochastic heterologous vaccination (Stoch-Hetero) Individuals in this category adjust their vaccination choices through a parallel minority game theory. In contrast to the fixed strategy, these individuals adopt a stochastic strategy:[43] their decisions are driven by a dynamic probability function that embodies the principle of the "avoiding the majority" game (see Eq. (2) for the specific mathematical formulations). Specifically, individuals allocate selection probabilities across multiple vaccines. This process can be intuitively represented by a probability tree analogous to the "rock-paper-scissors" game (Fig. 2).

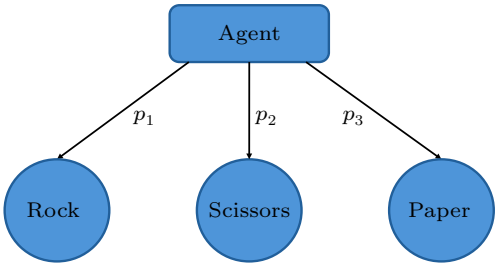


Fig. 2. Probability tree illustrating an individual's stochastic strategy in the 'rock–paper–scissors' game. The individual chooses rock, paper, or scissors with probabilities p_1, p_2, and p_3 ($p_1 + p_2 + p_3 = 1$).

(ii) Complete random heterologous vaccination (Rand-Hetero) Individuals are randomly assigned to receive any available vaccine type in the booster immunization stage, unaffected by parallel minority game theory. In the actual vaccination process, such completely random behavior is only likely to occur in a very small number of individuals. This study establishes it as a reference benchmark for the stochastic heterologous vaccination strategy, with comparisons being conducted to evaluate the impact of the parallel minority game decision-making mechanism on epidemic control effectiveness.

Next, we describe in detail the vaccination process of an individual during the booster phase of immunization. In order to clearly illustrate the dynamically coupled mechanism between individual vaccination decision and disease transmission, we first show the general logic and flow framework of the model in Fig. 3, and then explain each link step by step.

Step 1: Model initialization and basic assumptions

At the beginning of the simulation ($t = 0$), we consider a population of N individuals and D vaccine types, with the following fundamental assumptions:

(i) Primary immunization All individuals complete primary immunization and receive the same vaccine.

(ii) Regional heterogeneity The supply of vaccine types is unbalanced across regions. Following primary immunization, individuals may receive either a homologous or heterologous booster from the vaccines available locally.

(iii) Vaccine efficacy Each vaccine type has a different efficacy.

(iv) Decision grouping The population is split into a decision group (proportion h), which may adjust its choice based on game theory, and a non-decision-making group (proportion $(1-h)$), which is mandated to undergo homologous vaccination.

(v) One-time and irreversible decision Individuals allowed to switch vaccine types and had only one opportunity to make this choice during the entire booster vaccination stage. Once the decision is made and the booster dose is administered, it cannot be altered.

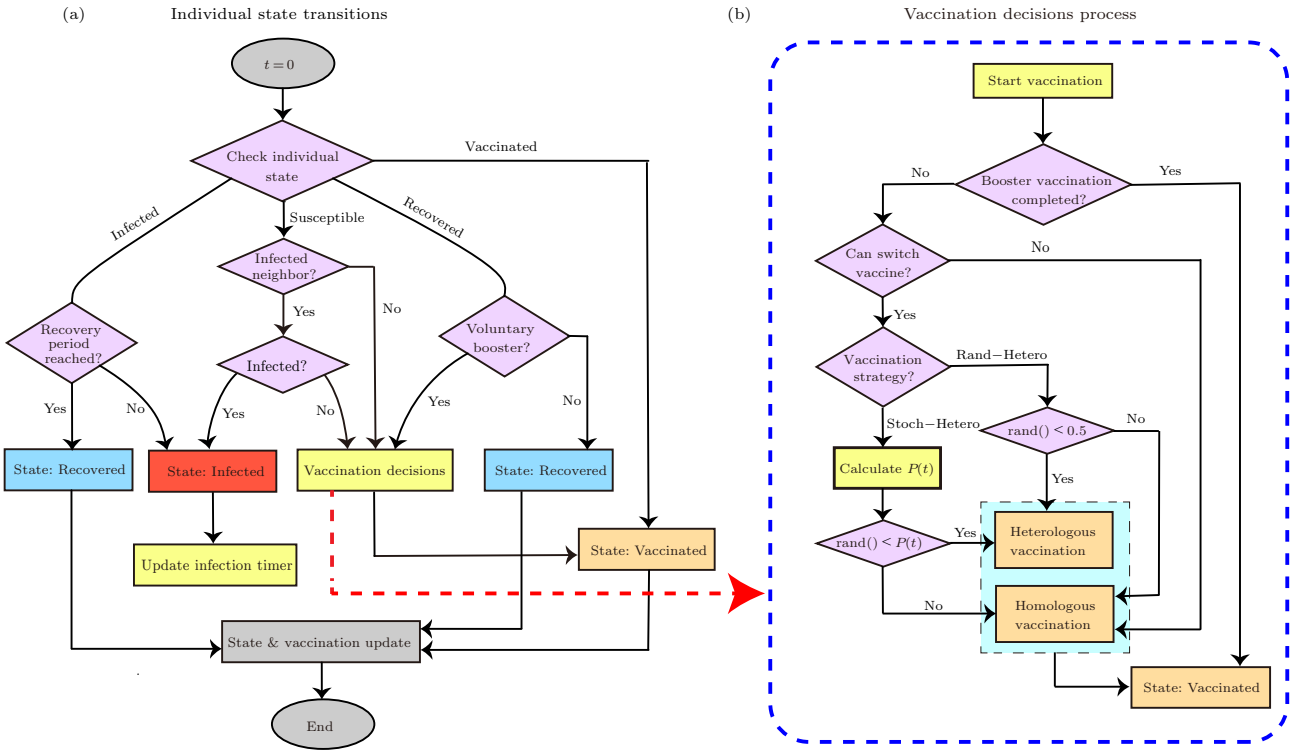


Fig. 3. Flowchart of the dynamic coupling mechanism between individual vaccination decisions and disease transmission. (a) Individual state transitions: the dynamic transitions of individuals among the susceptible, infected, recovered, and vaccinated states. (b) Vaccination decision process: the complete workflow of how individuals make decisions between homologous and heterologous booster vaccination strategies. The terms $P(t)$ (see Eq. (2)) and 0.5 in the figure denote the probability of an individual selecting a specific vaccine from the available types when adopting the stochastic and completely random strategies, respectively.

In summary, this study classifies individuals into a decision-making group (proportion h) and a non-decision-making group (proportion $1-h$) based on their autonomy in vaccination. Individuals in the decision-making group can choose between two vaccines during the booster phase, guided by real-time epidemic information and a parallel minority game, with only a single, irreversible decision opportunity. This PMG-based "herd-avoidance" behavior represents a form of strategic adaptation under limited information, applicable only to this subgroup, rather than depicting a general preference of the whole population. Non-decision-making individuals do not participate in selection and receive homologous boosters, continuing with the same vaccine used in primary immunization. This classification clarifies the differences in behavioral rules, decision constraints, and available strategies, providing a behavioral foundation for the coupled decision — epidemic dynamics modeling in subsequent chapters.

Step 2: Heterologous vaccination process for the decision group

As previously mentioned, heterologous vaccination strategies are categorized into two types: stochastic heterologous vaccination and completely random heterologous vaccination. This step will detail the implementation mechanisms for these two strategies within individuals in the decision group.

(1) Stochastic heterologous vaccination based on the parallel minority game.

Under conditions of information asymmetry, the judgment of the decision-pending (orange) individuals in Fig. 1 primarily relies on two types of observable public information: primarily the reinfection rate (V_m) and the number of recipients (N_m) of their current vaccine m, as well as the reinfection rate (V_n) of alternative vaccine n. However, critical information such as the actual number of recipients of alternative vaccines (N_n) and real-time decisions of other individuals remains inaccessible. Based on this incomplete information set, when an individual assesses that the reinfection rate of their current vaccine m exceeds that of alternative vaccine n (i.e., $V_m > V_n$), they classify themselves as part of a relatively disadvantaged majority group. At this point, their inclination to switch vaccines significantly increases. The probability that the σ-th individual in the majority group at time t switches vaccine types is given by the following formula:

$$P(t) = \frac{(V_m^\sigma N_m^\sigma - V_n^\sigma N_m^\sigma)/2}{hN_m^\sigma/(D-1)}, \quad V_m^\sigma > V_n^\sigma. \tag{2}$$

Here, m and n are the two vaccine options available to the σ-th individual. V_m^σ and V_n^σ are the reinfection rates of vaccines m and n. N_m^σ denotes the total number of individuals in the population who have chosen vaccine m at the current time step. The numerator term $(V_m^\sigma N_m^\sigma - V_n^\sigma N_m^\sigma)/2$ reflects the intensity of individuals' willingness to switch. This arises

because they perceive their currently selected vaccine as relatively disadvantaged compared to the majority. The denominator, $hN_m^{\sigma}/(D-1)$, acts as a normalization factor to ensure that the probability $P(t)$ remains within the range $[0,1]$. Its value corresponds to the average number of individuals that each of the remaining $D-1$ vaccine types would receive if all eligible switchers were evenly distributed among them.

Equation (2) constitutes the specific mathematical formulation of the stochastic strategy constructed in this study. Its ratio structure mathematically implements a self-regulating game mechanism. Individuals are encouraged to leave the majority. However, individuals' switching behavior is also constrained by the number of others with the same motivation and by the availability of alternative vaccine types. If all majority individuals move to the same expected minority option, a new majority is actually formed.

(2) Complete random heterologous vaccination.

This strategy serves as the benchmark reference for the stochastic heterologous vaccination strategy, simulating an individual's decision-making behavior without considering any epidemiological information. Each individual randomly selects one of the two available vaccines (where the total number of vaccine types $D > 2$) with a uniform probability of 0.5.

Upon completing the probability evaluation of the above strategies, both scenarios determine the final decision by comparing a randomly generated number $\varepsilon \in (0,1)$ with the corresponding probability value. If $\varepsilon \in (0,1)$ is less than the probability value, the individual decides to undergo heterologous vaccination; otherwise homologous vaccination is maintained. After making the decision, the individual immediately receives the booster vaccination, and their vaccine record is updated accordingly; this decision is final, and the individual no longer has the right to choose again during the entire booster vaccination stage.

Step 3: Disease transmission dynamics

Individuals' final vaccination decisions subsequently influence disease transmission dynamics. This study employs the Moore neighborhood to define the local contact network. For an individual at grid coordinates (i,j), their Moore neighborhood $N(i,j)$ comprises all eight directly adjacent cells in the horizontal, vertical, and diagonal directions surrounding the central cell. Formally, it is defined as

$$N(i,j) = \left\{ (i',j') \,\middle|\, |i-i'| \le 1,\ |j-j'| \le 1,\ (i',j') \ne (i,j) \right\},$$

where (i,j) represents the coordinates of an individual in the grid, and (i',j') represents the coordinates of its neighboring individuals.

Unlike the Von Neumann neighborhood, which includes only the four nearest neighbors (up, down, left, right), the Moore neighborhood additionally accounts for the four diagonal directions, thereby more realistically capturing potential contact patterns in space.

At any discrete time step, a susceptible individual may become infected only if there is at least one infected individual within their Moore neighborhood. Infected individuals transition to the recovered state after a fixed recovery period.

Step 4: Information update and cycle

At the end of each time step, the system globally updates all vaccines based on the latest infection and recovery data reinfection rates $(V_m, V_n, \ldots)$ and cumulative number of vaccinations $(N_m, N_n, \ldots)$. This real-time updated information forms the core basis for driving the game of decision-making individuals in the next time step.

In summary, this subsection defines a dynamic coupling process through the SIRV transmission model, the Moore neighborhood rule, and the parallel minority game. The process operates in discrete time steps: at time t, individual vaccination decisions are determined by the neighborhood epidemic state at time $t-1$; the collective effect of these decisions then drives the epidemic dynamics at time $t+1$. This discrete-time mechanism adopts a synchronous updating rule. Based on this coupling process, the next section will quantify and evaluate the effectiveness of different vaccination strategies through parameter settings and scenario design.

2.2. Parameter settings and experimental scenarios

With the vaccination strategies, individual decision-making processes, and transmission mechanism now established, the next step involves parameter configuration and experimental design to enable simulation implementation and evaluation of different intervention strategies.

2.2.1. Parameter configuration

Under the above framework, specific parameter assignments are required to implement the simulations. This subsection presents the configuration basis for grid parameters (population density ρ and grid side length L) and epidemiological parameters.

Population density ρ is one of the most critical factors in configuring grid parameters, as it directly reflects spatial contact structures. It directly determines the frequency of contact and transmission risk between susceptible and infected individuals within a neighborhood. Figure 4 visually illustrates the core mechanism driving this risk, namely, susceptible individuals (yellow) transforming into newly infected individuals (dark red) after contact with infected individuals (red) within their Moore neighborhood. Based on this observation, it can be inferred that when individuals are densely distributed, the probability of an infected individual appearing within the neighborhood of any susceptible individual is significantly increased, making new infections more likely to occur. Conversely, when the distribution is sparse, such effective contact opportunities are substantially reduced, thereby lowering the transmission risk.

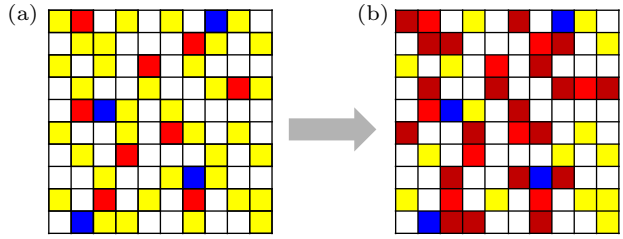


Fig. 4. Schematic diagram of the neighborhood infection mechanism on the grid. (a) Evolution of individual states at time t. (b) Evolution of individual states at time $t+1$. Yellow represents susceptible individuals, red represents initial infectives, blue represents recovered individuals, and dark red represents newly infected individuals at time $t+1$ resulting from the coexistence of infective sources and susceptibles within the neighborhood.

In order to rationally determine the critical value of population density ρ and reveal its key role in the propagation process, we introduce the percolation theory[44] as an analytical framework. According to percolation theory,[44] the critical density of occupied nodes (i.e., the percolation threshold) in the standard two-dimensional square lattice model is approximately $p_c \approx 0.5927$.[44] The liquidity phenomenon described by this threshold is consistent with the epidemic transmission patterns.[44–46] When population density approaches p_c, the contact network reaches a critical state that sustains local transmission but prevents global spread. This mechanism reflects the inhibitory effect of real-world interventions such as social distancing.[16,47] At this time, due to the spatial heterogeneity of population distribution,[48] the scope of epidemic transmission often shows a dynamically changing fractal structure.[49] The concept of connected clusters in percolation theory can be used to characterize this spatial aggregation and transmission threshold property:[44,49,50] when density exceeds a certain threshold, globally connected superclusters are likely to form, leading to widespread transmission; conversely, transmission chains are confined to localized areas.

Based on the aforementioned theory, we further determine the population density parameter ρ. We employ a susceptible–infected–recovered–vaccinated (SIRV) infectious disease model incorporating vaccinated populations to validate the critical regulatory role of the percolation threshold, thereby establishing the population density value suitable for subsequent simulations. In the simulation design, we fix the total population size ($N = 15000$), and adjust the spatial grid size to achieve different population density ρ conditions. Specifically, we select three representative scenarios for the SIRV dynamics simulation: below threshold ($\rho = 0.1 < p_c$), near threshold ($\rho = 0.5 \approx p_c$), and above threshold ($\rho = 0.9 > p_c$).

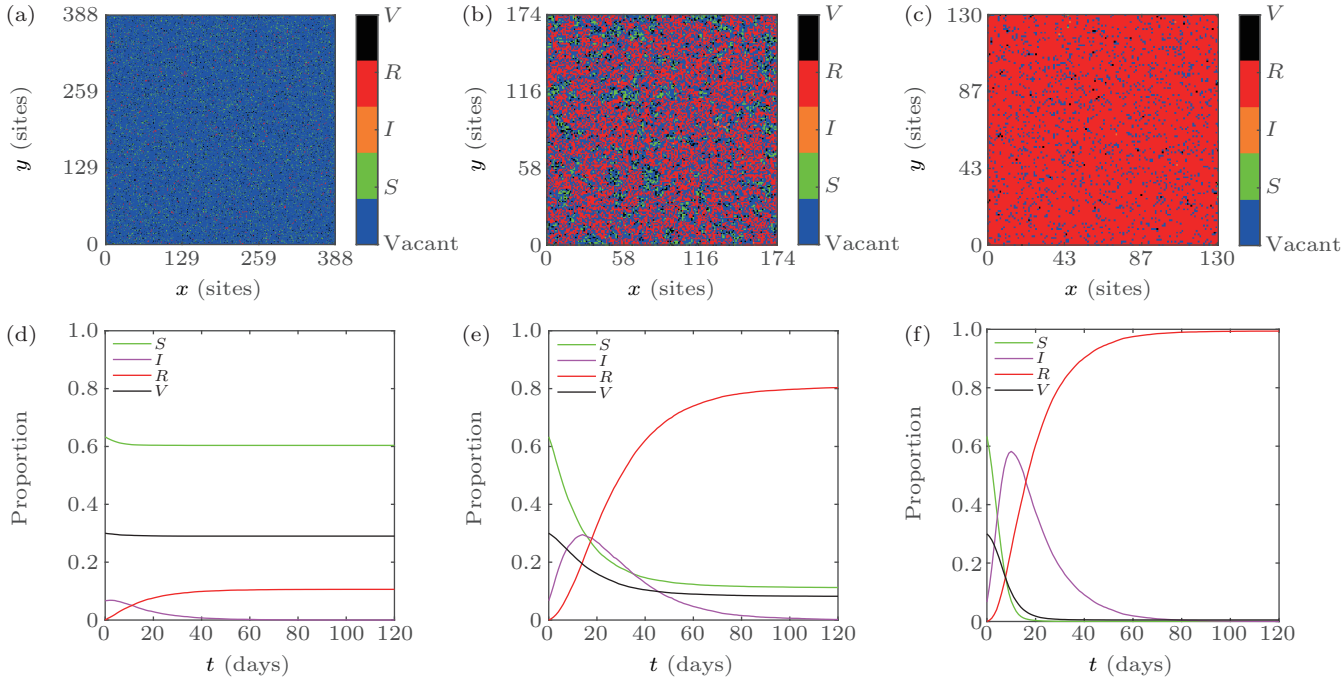


Fig. 5. Spatial patterns and dynamic evolution of epidemic transmission under different population densities. (a)–(c) Final lattice snapshots of the SIRV model simulations with grid side lengths of $L = 388, 174, 130$, corresponding to population densities of $\rho = 0.1, 0.5, 0.9$, respectively. (d)–(f) Dynamic evolution curves of each population group under the corresponding scenarios in panel (a)–(c). Color code for lattice: blue — vacant, green — susceptible (S), orange — infected (I), red — recovered (R), black — vaccinated (V). Color code for curves: green — S, magenta — I, red — R, black — V. In all simulations, the number of initial infected individuals is fixed at 1000.

Figures 5(a)–5(c) show lattice snapshots at the end of the SIRV model simulations under population densities $\rho = 0.1, 0.5, 0.9$, respectively, illustrating the impact of different densities on individual spatial distributions, and the number of sites corresponds to the lattice (grid) length; the corresponding dynamic evolution processes are shown in Figs. 5(d)–5(f). The lattice size L varies with the density ρ, as determined by Eq. (1), where the total population N is kept constant. Specifically, figure 5(a) shows that at a density of 0.1, the grid is predominantly composed of blue vacant sites, reflecting sparse

population distribution. In the corresponding Fig. 5(d), the number of infected individuals continues to decline, reaching zero by day 36, while the recovery rate remains only about 11%. This indicates that low density leads to rapid disruption of transmission chains. Figure 5(b) shows that at a density of 0.5, recovered individuals predominate in red; in the corresponding Fig. 5(e), the number of infected individuals rises slowly and peaks at about 28% on day 15, with the proportion of recovered individuals eventually stabilizing at about 78%. This indicates that when population density ρ approaches the threshold, vaccine intervention can effectively control the epidemic. In contrast, Fig. 5(c) shows that the lattice exhibits high clustering at a density of 0.9. In Fig. 5(f), the number of infected individuals surges sharply, peaking at about 56% by day 10, with a recovery rate ultimately reaching about 99.4%. This demonstrates that high density leads to rapid and uncontrolled spread of the epidemic.

Table 1. The simulation parameters on the two-dimensional grid.

Term	Meaning	Value	Reference
R_0	The basic reproductive number	1.4	[53]
β	Transmission rate from infectious individuals to susceptible individuals per day	0.1	Estimated
γ	Recovery rate from the infectious individuals to the recovered individuals (day^{-1})	1/14	[54,55]
v	Effectiveness of vaccine i in preventing infection	0.6–0.95	[42,51,52]
h	Proportion of individuals eligible to switch vaccine types among the total population N	(0–1)	Theoretical range
h_1	Proportion of individuals in state S eligible to switch vaccine types	(0–1)	Randomly sampled in simulations
h_2	Proportion of individuals in state R eligible to switch vaccine types	(0–1)	Randomly sampled in simulations
q	Proportion of individuals in state R who voluntarily receive booster immunization	0.2	[56]
$P(t)$	Probability that an individual chooses to switch vaccine types in booster immunization stage	(0–1)	Eq. (2)

The results above indicate that when population density

$$\rho = 0.5$$

(close to p_c), implementing interventions such as vaccination can effectively control epidemic transmission. From Eq. (1), the side length L of the square grid can be calculated as approximately

$$L = \sqrt{\frac{N}{\rho}} = \sqrt{\frac{15000}{0.5}} \approx 173,$$

where N is the total number of individuals. This grid size ensures that the network of individual contacts is strong enough to maintain the chain of transmission but strong enough to be effectively suppressed by intervention strategies such as vaccination. Therefore, this paper employs a grid with population density $\rho = 0.5$ and $L = 173$ to simulate disease transmission.

The parameter values used in the two-dimensional grid simulation are listed in Table 1.

2.2.2. Combinations of vaccine efficacy

After establishing the fundamental epidemiological parameters, the variation in vaccine efficacy emerges as a critical factor influencing the selection of containment strategies. To systematically evaluate the impact of this factor, this study designs two typical scenarios: large and small differences in vaccine effectiveness.

First, we determined the range of values for vaccine effectiveness based on existing clinical research. Studies have shown that vaccine efficacy is usually set in the range of 0.6 to 0.95, reflecting the actual differences between different technical routes: recombinant protein vaccines can achieve protection rates above 90%,[51] while inactivated or adenovirus vaccines mostly range between 60% and 80%.[42,52] This variation in efficacy directly affects booster strategies: when the difference is significant, heterologous boosting can enhance protection through complementary immune mechanisms; when the difference is small, homologous boosting offers advantages in operational convenience.

Then, based on the above range of values, we define the following two contrasting scenarios:

1. Large difference scenario The efficacies of the three vaccines are set at 0.6, 0.7, and 0.95, representing low, medium, and high levels of protection, respectively.

2. Small difference scenario Vaccine efficacies (VEs) are determined through random generation. The specific calculation formula is $VE_i = 0.6 + (0.95 - 0.6)u$, where $u \sim U(0,1)$ is a uniform random variable in the interval $[0,1]$, and i denotes the vaccine type.

3. Data-based mechanism validation and numerical simulation

3.1. Validation of the vaccination-transmission coupled mechanism based on real data

To validate the accuracy of the vaccination-transmission mechanism constructed based on parallel minority game (PMG), this study uses the spread of COVID-19 as an example, comparing actual observational data from the Our World in Data database[57] with simulated data generated based on this mechanism.

In order to accurately characterize the dynamics of epidemic transmission, the proportion of newly infected persons

was chosen as the core validation indicator in this section. This indicator can reflect changes in transmission more rapidly and is less disturbed by delays in data reporting and biases in mortality estimates.

In terms of parameter settings, considering that approximately 90% of China's population had completed primary vaccination and around 60% had received booster doses by December 2022, the proportion of individuals eligible for vaccine switching in the simulation is set to $h = 0.6$. To ensure consistent initial conditions, this study selects a time point when cumulative confirmed cases reach approximately 15000 per million population as the baseline for comparison. Based on this, we set the total simulated population to $N_{\text{sim}} = 10000$ and the initial number of infected individuals to $I_{\text{sim}}(0) = 150$.

Figure 6 presents a cross-validation result comparing the simulation outcomes based on the parallel minority game mechanism (green circles), actual observed data (red circles), and solutions of the mathematical model (blue curve). We will elaborate on the establishment and derivation process of the mathematical model in Subsection 4.3. All three datasets in Fig. 6 exhibit strongly consistent temporal patterns: the number of newly infected individuals increases continuously during the early stage of the epidemic, reaching its peak around day 30, and then gradually declines. By day 100 to day 120, the number of new infections approaches zero. Overall, all three curves demonstrate a rising trend followed by a gradual decline. We note that the simulation shows a slower decline than the actual data, possibly due to reporting delays during data collection.

The above comparative results consistently show that the coupled vaccine-transmission mechanism proposed in this paper can effectively reproduce the observed epidemiological dynamics. Based on this, the lattice simulation in Subsection 3.2 and the mean-field model in Section 4 are both based on empirical evidence, ensuring the reasonableness and credibility of the research conclusions.

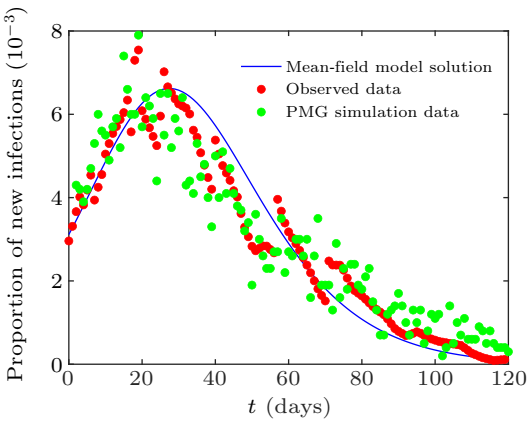


Fig. 6. Temporal evolution of the proportion of newly infected individuals. The blue solid line represents the solution to the mathematical model, the red circles represent the observed data, and the green circles represent simulation results based on PMG.

3.2. Analysis of key parameters on containment effectiveness

This section focuses on investigating the systemic impact of three key parameters: vaccine efficacy variation, the proportion of vaccine-switching individuals h, and the primary immunization level. Based on a two-dimensional grid, we select the following two core metrics for quantitative assessment: the time series of infected individuals, used to characterize the dynamic evolution and peak characteristics of the epidemic; the total number of infected individuals, used to measure the overall size of the transmission process.

3.2.1. Impact of vaccine efficacy combinations on vaccination strategy effectiveness

In this section, we systematically evaluate the epidemic mitigation performance of homologous vaccination, stochastic heterologous vaccination, and completely random heterologous vaccination strategies (Subsection 2.1) across scenarios characterized by either large or small disparities in vaccine efficacy.

In scenarios with large disparities in vaccine efficacy, with efficacies of 0.6, 0.7, and 0.95 for the three vaccines, different vaccination strategies exhibit distinct patterns of epidemic transmission (see Fig. 7). As shown in Fig. 7(a), the number of infected individuals under all three vaccination strategies — homologous vaccination (red curve), stochastic heterologous vaccination (green curve), and completely random heterologous vaccination (blue curve) — reaches a peak at time $t = 15$. However, significant differences exist in peak magnitude and decline rate: the completely random heterologous vaccination strategy exhibits the highest infection peak, followed by the homologous vaccination strategy, while the stochastic heterologous vaccination strategy shows the lowest peak (though with a slower decline in the epidemic). In terms of total number of infections (Figs. 7(b)–7(d)), stochastic heterologous vaccination (Fig. 7(c)) effectively reduces infection scale across different h values. Compared to homologous vaccination (Fig. 7(b)) and completely random heterologous vaccination (Fig. 7(d)), it reduces total infections by 34% and 39%, respectively. The latter two strategies consistently maintain higher levels of total infections.

The results above indicate that in scenarios where vaccine efficacy varies significantly, stochastic heterologous vaccination demonstrates superior control effects in reducing infection peaks and managing the overall scale of infections. This is mainly due to the following reasons: firstly, heterologous vaccination provides protection against a wider range of targets, offering individuals broader protective coverage compared to homologous vaccination; secondly, compared to completely random heterologous vaccination, stochastic heterologous vaccination introduces a parallel minority game mecha-

nism. Under the premise that vaccine efficacy exhibits clear superiority or inferiority, it fully accounts for the complex strategic behaviors of individuals during the vaccination process.

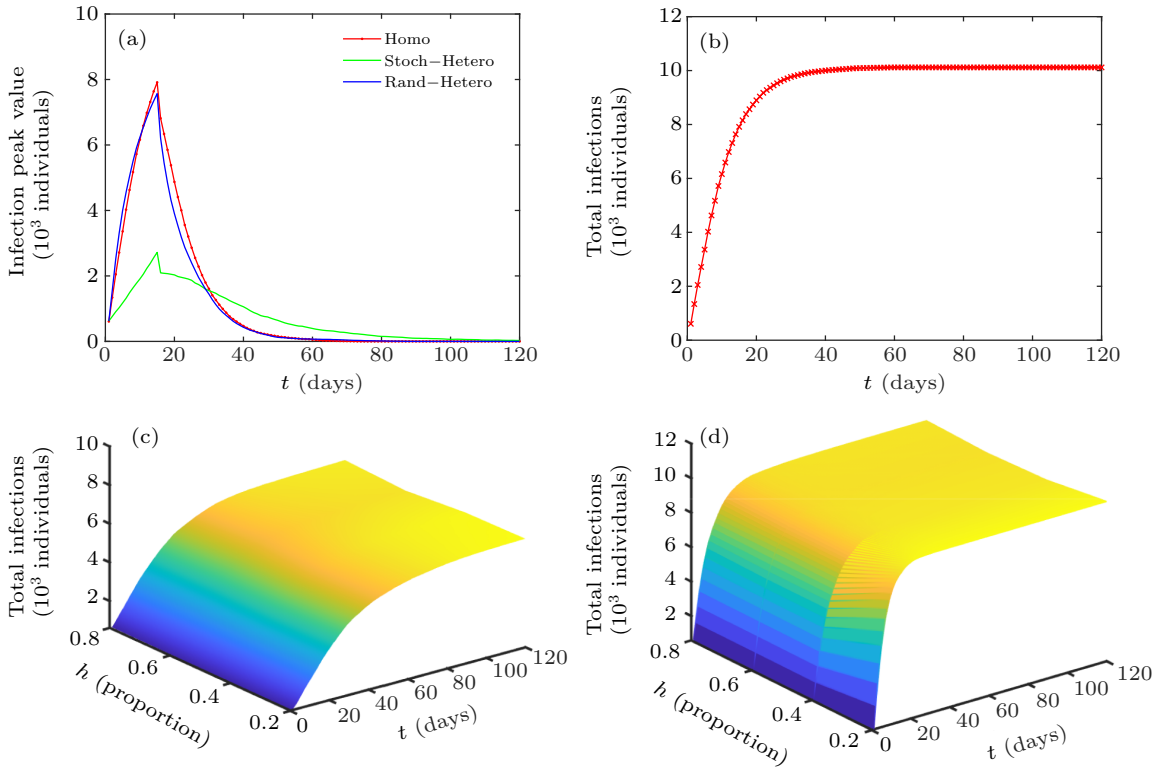


Fig. 7. Infection peak and total number of infections under different vaccination strategies when the difference in vaccine effectiveness is relatively large. Infection peak value indicates the peak number of infections at each time point, while the total infections refer to the total number of infections. (a) Temporal evolution of the number of infected individuals under different vaccination strategies. The red, green, and blue curves represent Homo, Stoch-Hetero, and Rand-Hetero, respectively. (b)–(d) Total number of infected individuals under different vaccination strategies: (b) Homo, (c) Stoch-Hetero, and (d) Rand-Hetero.

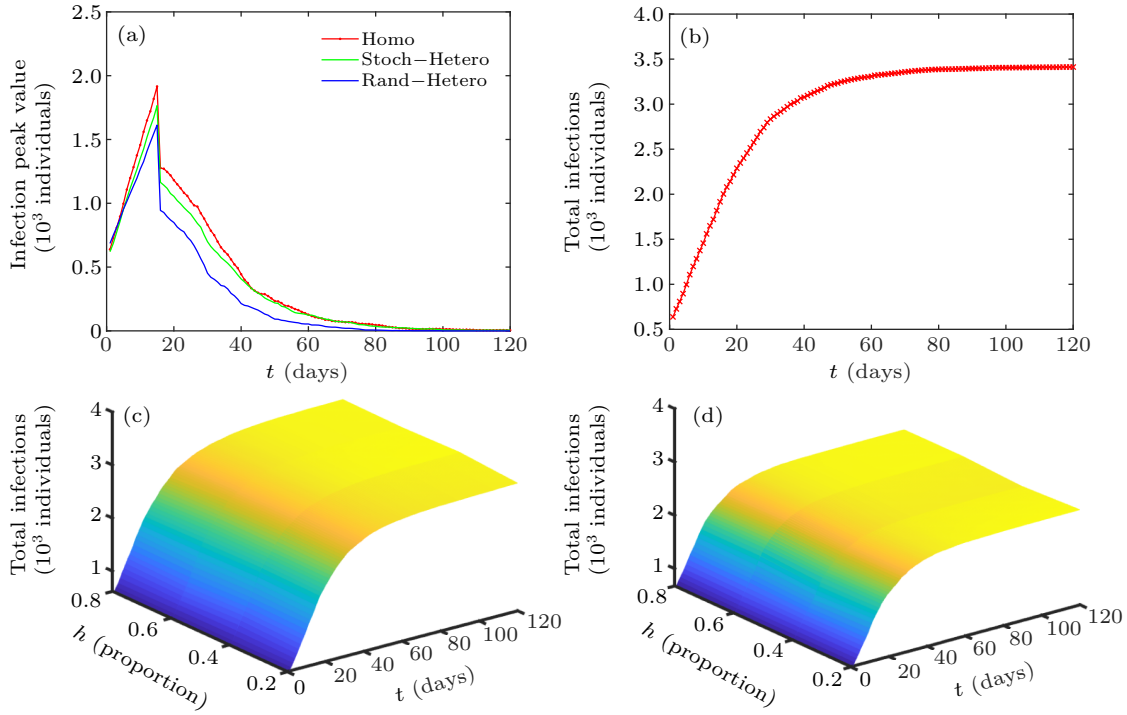


Fig. 8. Infection peak and total number of infections under different vaccination strategies when the difference in vaccine effectiveness is relatively large. Infection peak value indicates the peak number of infections at each time point, while the total infections refer to the total number of infections. (a) Temporal evolution of the number of infected individuals under different vaccination strategies. The red, green, and blue curves represent Homo, Stoch-Hetero, and Rand-Hetero, respectively. (b)–(d) Total number of infected individuals under different vaccination strategies: (b) Homo, (c) Stoch-Hetero, and (d) Rand-Hetero.

In scenarios with small disparities in vaccine efficacy (with $VE_i = 0.6 + (0.9 - 0.35)u$, $u \in [0, 1]$, see Fig. 8), the control efficacy of different vaccination strategies differs substantially from that under large vaccine efficacy disparities (Fig. 7). As shown in Fig. 8(a), the number of infected individuals under all three vaccination strategies reaches their peaks at the same time point $t = 15$. The peak number of infected individuals and the total number of infected individuals (Figs. 8(b)–8(d)) under the homologous vaccination strategy are higher than those under the heterologous vaccination strategy. Within the heterologous vaccination strategies, the completely random heterologous vaccination strategy performs slightly better than the stochastic heterologous vaccination strategy. The results indicate that when vaccine efficacy differences are small, although the advantage gap between different heterologous vaccination strategies narrows, their overall prevention and control effectiveness remains higher than that of the homologous vaccination strategy. This is primarily because: heterologous vaccination, by acting on different targets, forms a more comprehensive immune barrier compared to homologous vaccination. In the stochastic heterologous vaccination strategy , the parallel minority game mechanism makes it difficult to discern vaccine superiority due to converging efficacy rates. This leads individuals to make consistent choices under limited information, resulting in suboptimal clustering of vaccine types within populations. Consequently, the heterogeneity of the population's immune barrier is reduced. The completely random vaccination strategy, however, avoids interference from local information. Individuals select vaccine types purely at random, ensuring a uniform distribution of vaccine types across the population. This enhances the heterogeneity of the population's immune barrier, ultimately yielding slightly superior control outcomes.

The above results indicate that the degree of variation in vaccine effectiveness is a key regulatory factor determining the efficacy of vaccination strategies in disease control. Specifically: stochastic vaccination strategies outperform homologous vaccination; on this basis, when disparities are significant, stochastic heterologous vaccination demonstrates clear advantages in reducing infection peaks and controlling the overall scale of infections; when disparities are small, the parallel minority game mechanism fails due to the lack of a clear direction of superiority or inferiority. In such cases, the completely random heterologous vaccination strategy actually performs slightly better than the stochastic heterologous vaccination strategy.

3.2.2. Impact of vaccine switching proportion h under different heterologous vaccination strategies

The vaccine switching proportion h is a key parameter that reflects decision flexibility during booster vaccination. This parameter significantly regulates both the diversity of vaccination behaviors and the dynamics of disease transmission. After comparing the control effectiveness of different vaccination strategies under various vaccine efficacy combinations, we further examine the impact of parameter h (the proportion of individuals permitted to switch vaccine types) on both the stochastic heterologous vaccination and completely random heterologous vaccination strategies. Figure 7 illustrates how the infection peak and total number of infections vary under different values of h for the two strategies, specifically when vaccine efficacy differences are large and when they are small.

From Fig. 9(a), we can observe that under the stochastic heterologous vaccination strategy: when vaccine efficacy varies significantly (squares), the infection peak (blue) and total number of infected individuals (red) first decline gradually and then rise slightly as h increases, reaching their lowest values near $h = 0.6$. This suggests that an intermediate vaccine-switching rate optimally harnesses the benefits of heterologous vaccination, while an overly high value of h (i.e., allowing too many individuals to switch vaccines) could undermine the strategy's effectiveness. In contrast, when differences in vaccine efficacy are small, both the infection peak (green) and the cumulative number of infections (magenta) show little dependence on h.

In contrast, Fig. 9(b) shows that the results under the completely random strategy exhibit inconsistent trends. When vaccine efficacy varies significantly (squares), the peak number of infections (blue) and total infections (red) decrease markedly with increasing h, reaching an optimal value at $h = 0.6$ before slightly rebounding. This indicates that the completely random heterologous vaccination strategy is more sensitive to changes in h, with control effectiveness heavily dependent on the setting of h. When vaccine efficacy differences are small (circles), its performance resembles that of the stochastic heterologous vaccination strategy, with the infection scale unaffected by h values.

When the difference in vaccine effectiveness is large, the control effect reaches the optimal level at $h \approx 0.6$. This phenomenon reflects a crucial balance between immune diversity and collective decision-making: when h is too low, an insufficient number of individuals participate in heterologous vaccination, making it difficult to establish effective immune diversity; when h is too high, too many individuals tend to switch vaccines synchronously, leading to convergence in the population's immune structure. Both scenarios undermine control effectiveness. Thus, a moderate h value can maintain effective immune diversity while achieving optimal transmission control.

In summary, the superior performance of the stochastic heterologous vaccination strategy in most scenarios stems

from its introduction of a parallel minority game mechanism. This mechanism establishes coordination between individual choices and herd immunity, thereby demonstrating greater robustness when confronted with varying h values. In contrast, the completely random heterologous vaccination strategy lacks such a mechanism, making its control effectiveness susceptible to fluctuations in individual choice behavior and resulting in insufficient overall stability.

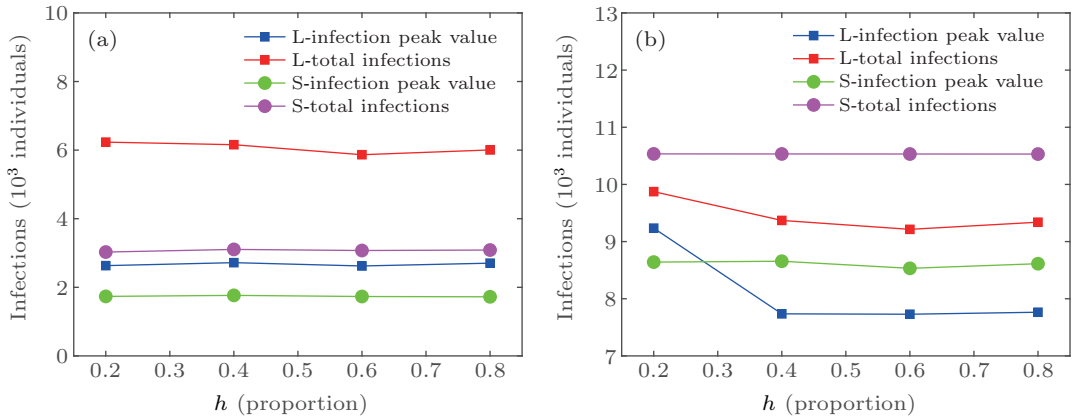


Fig. 9. Peak and total number of infections under different strategies as functions of the vaccine switching proportion h. (a) Peak and total infections versus h under the stochastic heterologous strategy. (b) Peak and total infections versus h under the completely random heterologous strategy. In the figure, blue squares (L-infection peak) and red squares (L-total infections) represent the peak number of infections and total infections, respectively, under the condition of large vaccine efficacy differences (L); green circles (S-infection peak) and magenta circles (S-total infections) represent the corresponding quantities under the condition of small vaccine efficacy differences (S).

3.2.3. Impact of vaccine efficacy heterogeneity in the primary immunization stage

A large majority of the population in China had completed primary vaccination by the first quarter of 2022.[58] Primary immunization, as the foundational stage of vaccination, critically shapes subsequent infection dynamics. In this subsection, we adopt a stochastic heterologous vaccination strategy, which mitigates the arbitrariness of completely random vaccination and overcomes the homogeneity constraints of homologous vaccination, thereby better capturing individuals' bounded rational behavior in vaccine selection. Based on this, we assess how different initial vaccine efficacy parameters affect the peak infection rate and total infections during epidemic transmission, with simulation results shown in Fig. 8.

Observing Fig. 10, when the vaccine efficacy during the primary immunization phase is 0.6 (red), 0.7 (magenta), 0.8 (blue), and 0.9 (green), respectively, it is evident that both the peak number of infections (Fig. 10(a)) and the total number of infections (Fig. 10(b)) show a decreasing trend as vaccine efficacy increases. This finding supports a classic epidemiological principle: building strong immunity early in an outbreak is key to controlling virus spread.[13,59] Therefore, when resources allow, using high-efficacy vaccines for primary immunization should be the core of outbreak control.

The aforementioned simulation results elucidate the impact of vaccine efficacy differences, the switching proportion h, and the level of primary immunization on epidemic control effectiveness. To gain a deeper understanding of the coupling mechanism between individual vaccination behavior and epidemic transmission dynamics observed in the simulations and to achieve its quantitative characterization, the next section will establish a mathematical model based on mean-field approximation.

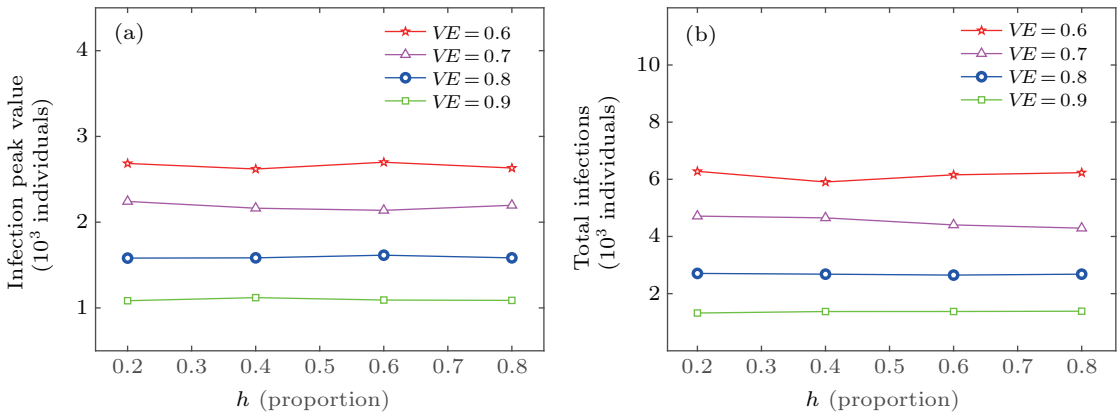


Fig. 10. (a) Infection peak as a function of the proportion of individuals eligible for vaccine switching under large vaccine effectiveness difference. (b) Total number of infections as a function of the proportion of individuals eligible for vaccine switching under the same conditions. The red, pink, blue, and green curves represent different levels of vaccine effectiveness.

4. Mean-field approximation

To simplify the structural complexity of the vaccination-transmission mechanism based on the parallel minority game in Section 2, we introduce a mean-field approximation and establish the corresponding ordinary differential equation model. This approach neglects local interactions between individuals and their neighbors, instead characterizing macroscopic dynamics through collective average behavior. This transformation converts complex local game processes into interactions between individuals and a global mean-field, thereby facilitating analysis.

The model is based on the following assumptions: (1) the total population remains constant; (2) births, natural deaths, and disease-related deaths are not considered. At the initial stage, all individuals are in the susceptible state.

4.1. Mean-field model formulation

This subsection aims to construct a mean-field model to describe, at the macroscopic scale, the vaccination decision mechanism based on parallel minority game presented in Section 2. By introducing a global mean-field to decouple individual dynamics, the model distills complex local game interactions into a unified evolutionary dynamical equation. Accordingly, we divide the total population into four compartments: susceptible (S), infected (I), recovered (R) and vaccinated (V). Here, the vaccinated compartment (V) includes individuals who have received both homologous and heterologous booster immunizations. These variables also represent the number of individuals in each corresponding state. Figure 11 shows the schematic diagram illustrating the epidemic dynamics during the booster immunization stage.

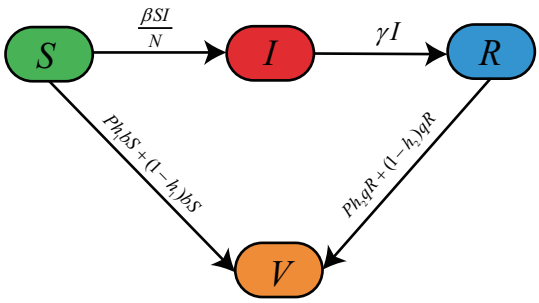


Fig. 11. Schematic diagram of the compartmental model for infectious disease transmission during the booster vaccination phase. S, I, R, V denote susceptible, infected, recovered, and vaccinated individuals, respectively. h_1 and h_2 represent the proportions of individuals in S and R who can switch vaccine types during the booster vaccination phase, respectively. b and q represent the proportions of vaccinated individuals in S and R, respectively. β is the infection rate, and γ is the recovery rate.

The key parameters of the model — the vaccine switching probability P, the proportion of susceptible individuals eligible to switch vaccines h_1, and the corresponding proportion among recovered individuals h_2 — are directly obtained from the simulations in Section 2. To simplify the analysis of macroscopic dynamics, this model incorporates the time-averaged values of these parameters as constant inputs, thereby finalizing the parameterizations of the mean-field model.

The dynamics of disease transmission during the booster stage are described by the following system of differential equations:

$$\begin{aligned}
\frac{\mathrm{d}S}{\mathrm{d}t} &= -\frac{\beta SI}{N} - Ph_1bS - (1-h_1)bS,\\
\frac{\mathrm{d}I}{\mathrm{d}t} &= \frac{\beta SI}{N} - \gamma I,\\
\frac{\mathrm{d}R}{\mathrm{d}t} &= \gamma I - Ph_2qR - (1-h_2)qR,\\
\frac{\mathrm{d}V}{\mathrm{d}t} &= Ph_1bS + (1-h_1)bS + Ph_2qR + (1-h_2)qR. \quad (3)
\end{aligned}$$

Here, h_1 and h_2 represent the proportions of individuals in S and R, respectively, who are allowed to switch vaccine types during the booster stage. b and q denote the proportions of individuals in S and R who receive vaccination. β is the infection rate, and γ is the recovery rate.

Through the above mean-field approximation, we transform complex individual heterogeneity and local interactions into average dynamic behavior at the population level. This approach preserves the core characteristics of the parallel minority game while significantly simplifying the analytical complexity of the model, providing a viable theoretical framework for studying the evolution of herd immunity.

4.2. Dynamical analysis

4.2.1. Well-posedness

Theorem 1 If the initial conditions of system (3) satisfy $S(0)\geq 0, I(0)\geq 0, R(0)\geq 0, V(0)\geq 0$, then for all $t>0$, the solutions $S(t), I(t), R(t), V(t)$ remain non-negative, i.e., $S(t), I(t), R(t), V(t)\geq 0$.

Proof From the equations

$$\begin{aligned}
\frac{\mathrm{d}S}{\mathrm{d}t} &= -\frac{\beta SI}{N} - bS\left[Ph_1 + (1-h_1)\right],\\
\frac{\mathrm{d}I}{\mathrm{d}t} &= \frac{\beta SI}{N} - \gamma I,
\end{aligned}$$

we have

$$S(t) = S(0)\exp\left(-\int_0^t \left(\frac{\beta I(\tau)}{N} + Ph_1b + (1-h_1)b\right)\mathrm{d}\tau\right), \quad (4)$$

$$I(t) = I(0)\exp\left(\int_0^t \left(\frac{\beta S(\tau)}{N} - \gamma\right)\mathrm{d}\tau\right). \quad (5)$$

Since the exponential function is always positive, if $S(0)>0$ and $I(0)>0$, then $S(t)>0$ and $I(t)>0$. If $S(0)=0$ and $I(0)=0$, then from the differential equations we have $\mathrm{d}S/\mathrm{d}t=0$ and $\mathrm{d}I/\mathrm{d}t=0$, hence $S(t)=0$ and $I(t)=0$. Therefore, $S(t)\geq 0$ and $I(t)\geq 0$.

From

$$\frac{\mathrm{d}R}{\mathrm{d}t} = \gamma I - qR\left[Ph_2 + (1-h_2)\right],$$

we get

$$\begin{aligned} R(t) \;=\; & R(0)\,\mathrm{e}^{-q(Ph_2+(1-h_2))t} \\ & + \int_0^t \gamma I(\tau)\,\mathrm{e}^{-q(Ph_2+(1-h_2))(t-\tau)}\,\mathrm{d}\tau. \end{aligned} \tag{6}$$

Since $R(0) \geq 0$, $I(\tau) \geq 0$, and the exponential function is positive, it follows that $R(t) \geq 0$.

Finally, from

$$\frac{\mathrm{d}V}{\mathrm{d}t} = bS\left[Ph_1 + (1-h_1)\right] + qR\left[Ph_2 + (1-h_2)\right],$$

integrating gives

$$\begin{aligned} V(t) \;=\; & V(0) + \int_0^t \big(b(1-h_1+Ph_1)S(\tau) \\ & + q(1-h_2+Ph_2)R(\tau)\big)\,\mathrm{d}\tau, \end{aligned} \tag{7}$$

where $1-h_1+Ph_1 \geq 0$ and $1-h_2+Ph_2 \geq 0$. Given that $b,q > 0$ and $S(\tau), R(\tau) \geq 0$, the integrand is nonnegative. Hence, $V(t) \geq V(0) \geq 0$.

Therefore, for all $t \geq 0$,

$$S(t) \geq 0, \quad I(t) \geq 0, \quad R(t) \geq 0, \quad V(t) \geq 0.$$

Theorem 2 Define the state vector $\boldsymbol{X}(t) = (S(t), I(t), R(t), V(t))^{\mathrm{T}}$. For any initial condition $\boldsymbol{X}(0) = \boldsymbol{X}_0 \in \mathbb{R}^4$, the system admits a unique solution $\boldsymbol{X} \in C^1([0,\infty);\mathbb{R}^4)$.

Proof System (3) can be expressed in the autonomous form

$$\frac{\mathrm{d}\boldsymbol{X}}{\mathrm{d}t} = \boldsymbol{F}(\boldsymbol{X}),$$

where

$$\boldsymbol{F} : \mathbb{R}^4 \to \mathbb{R}^4$$

is defined as

$$\boldsymbol{F}(\boldsymbol{X}) = \begin{pmatrix} -\frac{\beta SI}{N} - Ph_1 bS - (1-h_1)bS \\ \frac{\beta SI}{N} - \gamma I \\ \gamma I - Ph_2 qR - (1-h_2)qR \\ Ph_1 bS + (1-h_1)bS + Ph_2 qR + (1-h_2)qR \end{pmatrix}. \tag{8}$$

Each component of $\boldsymbol{F}(\boldsymbol{X})$ is a continuous polynomial function of the state variables, thus

$$\boldsymbol{F}(\boldsymbol{X}) \in C^{\infty}(\mathbb{R}^4;\mathbb{R}^4),$$

i.e., $\boldsymbol{F}$ is smooth. By the Picard–Lindelöf theorem, for any initial condition $\boldsymbol{X}_0 \in \mathbb{R}^4$, there exists a unique local solution $\boldsymbol{X}(t)$ defined on an interval $[0,T]$ with $T > 0$.

Define $N(t) = S(t) + I(t) + R(t) + V(t)$, then

$$\frac{\mathrm{d}N}{\mathrm{d}t} = \frac{\mathrm{d}}{\mathrm{d}t}(S+I+R+V) = 0,$$

so $N(t) \equiv N$ is constant, which implies total population is conserved. Since $S(t), I(t), R(t)$, and $V(t)$ are all non-negative and satisfy $S(t)+I(t)+R(t)+V(t) \equiv N$, each state variable is uniformly bounded on $[0,T]$:

$$0 \leq S(t), I(t), R(t), V(t) \leq N, \quad \forall t \in [0,T],$$

i.e., the solution is uniformly bounded. By the extension theorem for ordinary differential equations, the local solution can be extended globally, hence there exists a unique solution

$$\boldsymbol{X} \in C^1([0,\infty);\mathbb{R}^4).$$

4.2.2. Basic reproduction number

We use the next-generation matrix method to analyze the basic reproduction number R_0. Following the framework of van den Driessche and Watmough,[60] the system can be decomposed into two components: the new infection terms ($\mathcal{F}$) and the transition terms ($\mathcal{V}$), where the latter represents all state transitions other than new infections, including recovery.

The rate of new infections entering the infected compartment is

$$\mathcal{F} = \beta \frac{S(0)I}{N}.$$

The rate of transition out of the infected compartment (here only due to recovery) is

$$\mathcal{V} = \gamma I.$$

Taking the partial derivatives with respect to the infected variable I yields

$$F = \frac{\partial \mathcal{F}}{\partial I} = \beta \frac{S(0)}{N}, \quad V = \frac{\partial \mathcal{V}}{\partial I} = \gamma.$$

Then, the basic reproduction number is obtained as

$$R_0 = \rho(FV^{-1}) = \frac{\beta S(0)}{\gamma N}. \tag{9}$$

4.2.3. The final size

In the model constructed herein, individuals are categorized into four states: S, I, R, V. Although the nonlinear dynamics of the model make analytical solutions difficult to obtain, the ultimate epidemic size Z — that is, the total number of individuals who have accumulated in the infected state I by the end of the epidemic — can be defined through an integral equation.This integral equation requires numerical solution using MATLAB. Specifically, the ultimate size can be expressed as

$$Z = \int_0^{\infty} \frac{\beta S(t) I(t)}{N}\,\mathrm{d}t. \tag{10}$$

From the equation for S,

$$\frac{\mathrm{d}S}{\mathrm{d}t} = -S\left[\frac{\beta I}{N} + Ph_1 b + (1-h_1)b\right],$$

we obtain

$$S(0) - S(\infty) = \int_0^\infty \left[\frac{\beta SI}{N} + b(1-h_1+Ph_1)S\right] \mathrm{d}t.$$

Assuming $S(\infty) = 0$, we have

$$S(0) = Z + b(1-h_1+Ph_1)\int_0^\infty S(t)\,\mathrm{d}t. \tag{11}$$

Similarly, integrating the I equation gives

$$\int_0^\infty \left(\frac{\beta SI}{N} - \gamma I\right) \mathrm{d}t = I(\infty) - I(0) = -I(0),$$

so that

$$Z = -I(0) + \gamma \int_0^\infty I(t)\,\mathrm{d}t. \tag{12}$$

Let

$$L := \int_0^\infty I(t)\,\mathrm{d}t,$$

then

$$L = \frac{Z + I(0)}{\gamma}. \tag{13}$$

Define

$$M := \int_0^\infty S(t)\,\mathrm{d}t, \quad W := \int_0^\infty S(t)I(t)\,\mathrm{d}t, \tag{14}$$

we have the following system of integral identities:

$$\begin{cases} Z = \beta W, \\ S(0) = Z + b(1-h_1+Ph_1)M, \\ L = \dfrac{Z+I(0)}{\gamma}. \end{cases} \tag{15}$$

To express Z in terms of parameters and initial conditions only, W or M can be eliminated using the analytic solution of $S(t)$. Substituting into the definition of Z, we obtain

$$Z = \frac{\beta S(0)}{N}\int_0^\infty I(t) \times \exp\left[-\frac{\beta}{N}\int_0^t I(s)\,\mathrm{d}s - b(1-h_1+Ph_1)t\right] \mathrm{d}t. \tag{16}$$

Let

$$u(t) := \int_0^t I(s)\,\mathrm{d}s, \quad u \in [0, L], \quad \mathrm{d}u = I(t)\,\mathrm{d}t,$$

with $u(\infty) = \frac{Z+I(0)}{\gamma}$. Changing the integration variable from t to u yields

$$Z = \frac{\beta S(0)}{N}\int_0^L \exp\left[-\frac{\beta}{N}u - b(1-h_1+Ph_1)T(u)\right] \mathrm{d}u, \tag{17}$$

where $T(u)$ is the inverse function of $u(t)$, i.e., the time when the cumulative number of infections reaches u, satisfying $T(0) = 0$ and $T(L) = \infty$.

The final size is defined by the integral equation (Eq. (17)). Due to the difficulty in obtaining its analytical solution, numerical methods are typically required for its determination. This work focuses on mechanism modeling and framework construction; therefore, the numerical solution process is not elaborated upon.

4.3. Validation of the coupled mechanism based on mean-field approximation

In Subsection 3.1, we conducted preliminary validation of the vaccination-transmission mechanism based on the parallel minority game (PMG) using actual observational data (see Fig. 6). This section will further validate this mechanism using a mathematical model based on the mean-field approach, building upon the parameters established in Subsection 3.1 (see Fig. 6).

Based on the initial conditions of the mean-field model, $N_{\mathrm{model}} = 21860$, $I_{\mathrm{model}}(0) = 400$, we determined the key kinetic parameters through least-squares fitting of the actual observational data in Fig. 6: infection rate $\beta = 0.1760$, recovery rate $\gamma = 0.1110$. As shown in Fig. 6, the simulation results based on the parallel minority game mechanism, the solutions from the mathematical model, and the actual observational data all exhibit highly consistent trends. This confirms the validity of the constructed vaccination-transmission mechanism.

5. Discussion and conclusion

Under the context of infectious disease outbreaks, the use of multi-platform vaccines has gradually highlighted the advantages of heterologous vaccination. Compared with homologous vaccination, which targets a single antigen and establishes a single immune barrier in the population, heterologous vaccination can target multiple antigens, thereby establishing a more comprehensive immune barrier at the population level. The effectiveness of this strategy, however, largely depends on individual vaccination decisions, and the underlying decision-making mechanisms under conditions of incomplete information are still unclear. Conventional game theory, constrained by perfect rationality assumptions or binary choice frameworks, fails to adequately capture the majority-avoidance behavior in individual vaccine selection. In contrast, the parallel minority game (PMG) theory can characterize the strategic choices made by individuals with bounded rationality in scenarios involving multiple vaccines. To address the aforementioned issues, this paper constructs a coupled dynamic framework of infectious disease transmission incorporating vaccination, based on a parallel minority game. This framework characterizes the decision-making process of boundedly rational

individuals in scenarios with multiple vaccines under conditions of incomplete information, thereby integrating vaccination decisions and disease transmission within a unified analytical framework. Within this framework, we define three vaccination strategies: homologous vaccination (Homo), stochastic heterologous vaccination (Stoch-Hetero), and completely random heterologous vaccination (Rand-Hetero). We simulate the vaccination-transmission process on a two-dimensional grid, with results indicating that heterologous vaccination yields superior overall control efficacy compared to homologous vaccination.

To validate the accuracy of the mechanism described above, we first compare simulation data based on parallel minority game (PMG) with actual observational data (using COVID-19 as an example). As shown in Fig. 6, the trends exhibit high consistency, which provides preliminary validation for the effectiveness of the vaccination-transmission coupling mechanism constructed in this paper. Based on the above mechanism, we further show differences in vaccine efficacy, the proportion h of vaccine-replaceable individuals, and the vaccine efficacy during the baseline immunization phase on the overall prevention and control effectiveness: (i) different combinations of vaccine effectiveness have a significant effect on the effectiveness of the vaccination strategies. When the differences in vaccine effectiveness are large, the stochastic heterologous vaccination (Stoch-Hetero) outperforms the other two strategies in reducing the peak and total number of infections (see Fig. 7); when the differences are small, heterologous vaccination (Hetero) still outperforms homologous vaccination (Homo), while the completely random heterologous vaccination (Rand-Hetero) strategy performs slightly better than the stochastic heterologous vaccination (Stoch-Hetero) strategy (see Fig. 8); (ii) the parallel minority game mechanism endows the stochastic heterologous vaccination (Stoch-Hetero) strategy with significant robustness advantages. Specifically, when vaccine efficacy varies considerably, its control effectiveness reaches an optimal level around an individual replacement rate of $h = 0.6$ and remains insensitive to parameter changes. In contrast, the control effectiveness of the completely random heterologous vaccination strategy (Rand-Hetero) exhibits instability (see Fig. 9); (iii) under the stochastic heterologous vaccination (Stoch-Hetero), the higher the vaccine effectiveness in the basic immunization phase, the better the control and prevention (see Fig. 10). To further validate the aforementioned mechanism, we simplify it into an ordinary differential equation model based on the mean-field approximation (Eq. (3)). Subsequently, we conduct a theoretical analysis of the model, including its well-posedness, the derivation of the basic reproduction number R_0, and the calculation of the final epidemic size. Finally, we confirm the accuracy of the vaccination-transmission coupled mechanism based on the parallel minority game from a mean-field perspective by showing that the solutions of the mathematical model closely match the empirical data in Fig. 6.

This study establishes a vaccination-transmission coupled mechanism based on a parallel minority game, which captures the vaccination decisions of boundedly rational individuals. Specifically, this "mainstream avoidance" behavior within the model corresponds to a real-world decision-making logic: when individuals perceive a risk from a homogeneous immune barrier, they may proactively choose different vaccines to mitigate infection risk. The mechanism uncovers how micro-level choices shape macro-level transmission dynamics, offering a scientific basis for public health policymaking in multi-vaccine settings. Our findings suggest that, during the outbreak phase of infectious diseases, heterologous vaccination should be prioritized to leverage its advantage in building a comprehensive immune barrier, while prevention and control strategies should be flexibly adjusted in light of key factors such as differences in vaccine efficacy. Beyond common infectious diseases such as influenza and hepatitis B, the proposed framework also provides valuable guidance for evaluating vaccine strategies against emerging pathogens, like monkeypox and potential future epidemic threats.[61,62]

However, there are still some limitations in this study: the model has not fully considered the dynamic characteristics of vaccine effectiveness decay over time, and has not incorporated realistic factors such as vaccine safety and vaccination convenience; at the same time, the individual decision-making mechanism has not sufficiently integrated the influence of social factors such as media publicity. In the future, we can further introduce time-varying parameter mechanisms to depict the dynamic decay process of vaccine effectiveness, and to construct a quantitative weighting model of media influences in individual decision-making to enhance the explanatory power of the model regarding the complex system in reality.

Acknowledgment

Project supported by the National Natural Science Foundation of China (Grant Nos. 12571549, 12571592, 12471463, 12022113, and 12101573).

References

[1] Beyer W E, de Bruijn I A, Palache A M, Westendorp R G and Osterhaus A D 1999 *Arch. Intern. Med.* **159** 182
[2] World Health Organization 1980 *Wkly. Epidemiol. Rec.* **55** 145
[3] Henderson D A 2009 *Smallpox: The Death of a Disease: The Inside Story of Eradicating a Worldwide Killer* (Amherst, NY: Prometheus Books)
[4] Damijan J P, Damijan S and Kostevc Č 2022 *Vaccines* **10** 678
[5] Voysey M, Clemens S A C, Madhi S A, *et al.* 2021 *Lancet* **397** 99
[6] Zeng G, Wu Q, Pan H, *et al.* 2022 *Lancet Infect. Dis.* **22** 483

[7] Liu X, Shaw R H, Stuart A S V, *et al.* 2021 *Lancet* **398** 856
[8] Munro A P S, Janani L, Cornelius V, *et al.* 2021 *Lancet* **398** 2258
[9] Barros-Martins J, Hammerschmidt S I, Cossmann A, *et al.* 2021 *Nat. Med.* **27** 1525
[10] Sun G Q, He R Z, Hou L F, Luo X F, Gao S P, Chang L L, Wang Y and Zhang Z K 2025 *Phys. Rep.* **1111** 1–64
[11] Luo X F, He R Z, Hou L F, Gao S P, Jin Z, Sun G Q, Chang L L, Minati L and Boccaletti S 2025 *Phys. Rev. Res.* **7** 013262
[12] Huo L A and Wu B J 2024*Chin. Phys. B* **33** 038702
[13] Anderson R M and May R M 1991 *Infectious Diseases of Humans: Dynamics and Control* (Oxford: Oxford University Press)
[14] Hethcote H W 2000 *SIAM Rev.* **42** 599
[15] Diekmann O, Heesterbeek J A P and Britton T 2012 *Mathematical Tools for Understanding Infectious Disease Dynamics* (Princeton: Princeton University Press)
[16] Ferguson N M, Laydon D, Nedjati-Gilani G, *et al.* 2020 *Impact of Non-Pharmaceutical Interventions to Reduce COVID-19 Mortality and Healthcare Demand* (London: Imperial College COVID-19 Response Team)
[17] Zheng Y Y, Wang Z P, Sun Y N, Xie S J and Wang L 2025*Chin. Phys. B* **34** 100201
[18] Moghadas S M, Vilches T N, Zhang K, Wells C R, Shoukat A, Singer B H, Meyers L A, Neuzil K M, Langley J M, Fitzpatrick M C and Galvani A P 2021 *Clin. Infect. Dis.* **73** 2257
[19] Bauch C T and Earn D J D 2004 *Proc. Natl. Acad. Sci. USA* **101** 13391
[20] Reluga T C 2010 *PLoS Comput. Biol.* **6** e1000793
[21] Fenichel E P, Castillo-Chavez C, Ceddia M G, Chowell G, Parra P A G, Hickling G J, Holloway G, Horan R, Morin B, Perrings C, Springborn M, Velazquez L and Villalobos C 2011 *Proc. Natl. Acad. Sci. USA* **108** 6306
[22] Huo L A and Yin L Y 2025*Chin. Phys. B* **34** 068902
[23] Luo X F, Sun G Q, He R Z, Jin Z, Asamoah J K K, Xue Y and Chang L L 2024 *Chaos* **34** 073114
[24] Galvani A P, Reluga T C and Chapman G B 2007 *Proc. Natl. Acad. Sci. USA* **104** 5692
[25] Perisic A and Bauch C T 2009 *PLoS Comput. Biol.* **5** e1000280
[26] Simon H A 1955 *Q. J. Econ.* **69** 99
[27] Osborne M J and Rubinstein A 1994 *A Course in Game Theory* (Cambridge: MIT Press)
[28] Fu F, Rosenbloom D I, Wang L and Nowak M A 2011 *Proc. R. Soc. B* **278** 42
[29] Bauch C T and Bhattacharyya S 2012 *PLoS Comput. Biol.* **8** e1002452
[30] Hofbauer J and Sigmund K 1998 *Evolutionary Games and Population Dynamics* (Cambridge: Cambridge University Press)
[31] Nowak M A and Sigmund K 2004 *Science* **303** 793
[32] Sandholm W H 2010 *Population Games and Evolutionary Dynamics* (Cambridge: MIT Press)
[33] Challet D and Zhang Y C 1997 *Physica A* **246** 407
[34] Challet D, Marsili M and Zhang Y C 2000 *Physica A* **276** 284
[35] De Martino A, Marsili M and Zhang Y C 2004 *Physica A* **332** 433
[36] Biswas S and Mandal A K 2021 *Physica A* **561** 125271
[37] Ranadheera S, Maghsudi S and Hossain E 2017 *IEEE Wirel. Commun.* **24** 184
[38] He R Z, Luo X F, Asamoah J K K, Zhang Y X, Li Y H, Jin Z and Sun G Q 2023 *J. Math. Biol.* **87** 29
[39] Yao D, Patel R S, Lam A, Glover Q, Srinivasan C, Herchen A, Ritchie B and Agrawal B 2024 *J. Virol.* **98** e01983-23
[40] Zhang X, Xia J, Jin L, Wu Y, Zheng X, Cao X, Meng X, Li J and Zhu F 2023 *Hum. Vaccines Immunother.* **19** 2236459
[41] Au WY, Cheung PP 2022 *Br. Med. J.* **377** e069989
[42] Jara A, Undurraga E A, González C, Paredes F, Fontecilla T, Jara G, Pizarro A, Acevedo J, Leo K, Leon F, Sans C, Leighton P, Suárez P, García-Escorza H and Araos R 2021 *N. Engl. J. Med.* **385** 875
[43] Dhar D, Sasidevan V and Chakrabarti B K 2011 *Physica A* **390** 3477
[44] Stauffer D and Aharony A 2018 *Introduction to Percolation Theory* 2nd edn (Boca Raton: Taylor & Francis)
[45] Khaleque A and Sen P 2017 *Sci. Rep.* **7** 42594
[46] Pastor-Satorras R, Castellano C, Van Mieghem P and Vespignani A 2015 *Rev. Mod. Phys.* **87** 925
[47] Haug N, Geyrhofer L, Londei A, Dervic E, Desvars-Larrive A, Loreto V, Pinior B, Thurner S and Klimek P 2020 *Nat. Hum. Behav.* **4** 1303
[48] Chang S, Pierson E, Koh P W, Gerardin J, Redbird B, Grusky D and Leskovec J 2021 *Nature* **589** 82
[49] Batty M and Longley P A 1994 *Fractal Cities: A Geometry of Form and Function* (London: Academic Press)
[50] Rhodes C J and Anderson R M 1996 *J. Theor. Biol.* **180** 125
[51] Dai L, Gao L, Tao L, *et al.* 2022 *N. Engl. J. Med.* **386** 2279
[52] Halperin S A, Ye L, MacKinnon-Cameron D, Smith B, Cahn P E, Ruiz-Palacios G M, Ikram A, Lanas F, Lourdes Guerrero M, Muñoz Navarro S R, Sued O, Lioznov D A, Dzutseva V, Parveen G, Zhu F, Leppan L, Langley J M, Barreto L, Gou J, Zhu T and CanSino COVID-19 Global Efficacy Study Group 2022 *Lancet* **399** 237
[53] Kucharski A J, Russell T W, Diamond C, *et al.* 2020 *Lancet Infect. Dis.* **20** 553
[54] Lai S, Ruktanonchai N W, Zhou L, Prosper O, Luo W, Floyd J R, Wesolowski A, Santillana M, Zhang C, Du X, Yu H and Tatem A J 2020 *Nature* **585** 410
[55] Weldu A, Asres A, Ayenew M, Michael T G, Giorgis T T, Mariam T G, Hiwot T G, Araya H, Silassie F G, Eyasu A G, Kirstos H G, David A G, Kiros T G, Tekle H G, Medhin T G, Haile T G, Abadi T G, Yohannes T G, Tadesse T G and Hagos T G 2025 *J. Public Health (Berl.)* **33** 513–519
[56] Zhang Z, Mateus J, Coelho C H, Dan J M, Moderbacher C R, Gálvez R I, Cortes F H, Grifoni A, Tarke A, Chang J, Escarrega E A, Kim C, Goodwin B, Bloom N I, Frazier A, Weiskopf D, Sette A and Crotty S 2022 *Cell* **185** 2434–2451
[57] https://ourworldindata.org/coronavirus
[58] https://www.peopleapp.com/column/30035597215-500004915582
[59] Keeling M J and Rohani P 2008 *Modeling Infectious Diseases in Humans and Animals* (Princeton: Princeton University Press)
[60] Van den Driessche P and Watmough J 2002 *Math. Biosci.* **180** 29–48
[61] Yuan P, Tan Y, Yang Z, Aruffo E, Ogden N H, Bélair J, Arino J, Heffernan J M, Watmough J, Carabin H and Zhu H 2022 *Front. Public Health* **10** 1026489
[62] Xiong Z X, Xue L, Li X Z and Zhang Y F 2024 *BMC Infectious Diseases* **24** 1078